

involve

a journal of mathematics

Numerical results on existence and stability
of steady state solutions for the reaction-diffusion
and Klein–Gordon equations

Miles Aron, Peter Bowers, Nicole Byer, Robert Decker,
Aslihan Demirkaya and Jun Hwan Ryu



Numerical results on existence and stability of steady state solutions for the reaction-diffusion and Klein–Gordon equations

Miles Aron, Peter Bowers, Nicole Byer, Robert Decker,
Aslihan Demirkaya and Jun Hwan Ryu

(Communicated by John Baxley)

In this paper, we study numerically the existence and stability of the steady state solutions of the reaction-diffusion equation, $u_t - au_{xx} - u + u^3 = 0$, and the Klein–Gordon equation, $u_{tt} + cu_t - au_{xx} - u + u^3 = 0$, with the boundary conditions: $u(-1) = u(1) = 0$. We show that as a varies, the number of steady state solutions and their stability change.

1. Introduction

Reaction-diffusion systems are mathematical models which describe the density/concentration of a substance, a population, etc. The typical form is

$$u_t = a\Delta u + f(u), \tag{1}$$

where $u(x, t)$ is the state variable at position x and at time t . Δu is the diffusion term with the diffusion constant a , and $f(u)$ is the reaction term.

To motivate [Equation \(1\)](#), consider letting $a = 0$, and $f(u) = ku$, and we get perhaps the simplest population growth ordinary differential equation $u_t = ku$. Here u represents the size of a population at time t which is growing with instantaneous growth rate k . Now imagine taking a one-dimensional spatially distributed population (such as fish in a long, narrow river) and sectioning it into N subpopulations lined up along the length of the river, each obeying $u_t = ku$. In this case, the fish from one subpopulation cannot move to an adjacent subpopulation. When we add the assumption that the fish can move between adjacent subpopulations and in fact will tend to move from more dense to less dense neighboring subpopulations (as is the case with diffusion), and taking the limit as $N \rightarrow \infty$, a one-dimensional linear reaction-diffusion equation $u_t = ku + au_{xx}$ is obtained. The au_{xx} term has the

MSC2010: 35B30, 35B32, 35B35, 35K57, 35L71.

Keywords: reaction-diffusion, Klein–Gordon equation, stability, steady state solutions.

effect of limiting growth at point x if $u(x, t)$ is concave down as a function of x (for fixed t) at that point (a assumed positive). Thus for example, if the neighbors of a subpopulation have smaller population densities, that subpopulation will tend to grow smaller due to emigration.

Thus we take the point of view that we can start with a standard dynamical system represented by a first-order differential equation and convert it into a distributed system represented by a partial differential equation by adding a diffusion term au_{xx} . The situation is similar with dynamical systems represented by second-order differential equations. For example, the equation for a damped mass-spring equation (with no driving force) is well known to be $mu_{tt} + cu_t + ku = 0$, where u represents the displacement from rest of a mass attached to a fixed point by a spring and damper as a function of time t , and m , c , and k are parameters representing the mass, the damping constant and the spring constant, respectively. By adding a diffusion term, we get the standard linear Klein–Gordon equation $mu_{tt} + cu_t + ku = au_{xx}$, which one can imagine to be a series of (vertical) harmonic oscillators tied together (horizontally) by more springs.

In this paper we are concerned with nonlinear systems, so in the case of the reaction-diffusion equation, instead of starting with the linear differential equation $u_t = ku$ we start with the nonlinear one: $u_t = u - u^3$ (which has stable fixed points at $u = \pm 1$ and an unstable fixed point at $u = 0$). This could be a model of a population with two stable values (after rescaling). This is similar to the example based on the classic spruce-budworm model studied in [Khain et al. 2010]. Converting this ODE to a PDE with the recipe of adding a diffusion term, we get the reaction-diffusion equation known as the Allen–Cahn equation:

$$u_t = au_{xx} + u - u^3. \quad (2)$$

For the case of the mass-spring system, we replace the linear restoring force by a nonlinear force of the form $f(u) = \alpha u + \beta u^3$ and end up with the Duffing equation:

$$u_{tt} + cu_t + \alpha u + \beta u^3 = 0, \quad (3)$$

where c is damping, and α and β are chosen so as to model various physical systems. For example, if α is negative and β is positive, the force tends to move the mass away from $u = 0$ and towards $u = \pm 1$ (one system with this property would be when magnets are added above and below the mass, which is assumed to be, say, made of iron, so that the mass is pulled from its equilibrium position either up or down, see Figure 1). Again, adding a diffusion term we get a nonlinear Klein–Gordon equation:

$$u_{tt} + cu_t + \alpha u + \beta u^3 = au_{xx}, u(-1) = u(1) = 0. \quad (4)$$

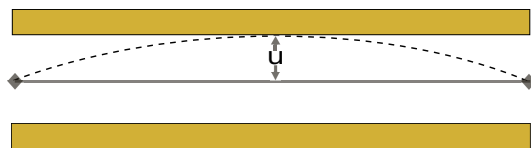


Figure 1. Damped, thin metal wire, fixed at $x = \pm 1$, placed between two magnets at $u = \pm 1$.

In both equations above when the parameter a is very small, we are back to a bunch of unconnected one-dimensional systems behaving independently. For the fish population in a river model, this would represent the idea that the fish could not migrate up or down the river, but can only reproduce and/or die in one location. For the mass-spring system this would represent totally unconnected, side-by-side oscillators with magnets. Thus we refer to a as the *strength of connection* parameter.

In this paper, by using *spectral methods*, we study the numerical existence and the stability of the steady state solutions of reaction-diffusion equation:

$$u_t = au_{xx} + u - u^3 \quad (5)$$

and Klein–Gordon equation:

$$u_{tt} + cu_t = au_{xx} + u - u^3. \quad (6)$$

For both cases we take the boundary conditions as $u(-1) = u(1) = 0$. We show that as a varies, the number of those special solutions and their stability change.

2. Spectral methods

Introduction. Because of the nonlinear terms added to our second order partial differential equations, we chose to use a numerical method of analysis instead of finding exact solutions. We used spectral methods of analysis (see [Trefethen 2000]) instead of more traditional methods, such as finite differences, due to the exponential order of error convergence that the spectral methods demonstrate.

Spectral methods break the second order partial differential equation into a series of first order differential equations. Each first order differential equation lies at a point called a Chebyshev point, which is similar to the equally spaced points used in finite differences. However Chebyshev points are selected by taking the x -coordinates of equally spaced points on a half-circle [Figure 2](#), top.

Chebyshev points are closer together towards the endpoints of the equation, which provides a much better polynomial fit and therefore much greater accuracy compared to equally spaced points as seen in [Figure 2](#), bottom (reproduced from [Trefethen 2000]).

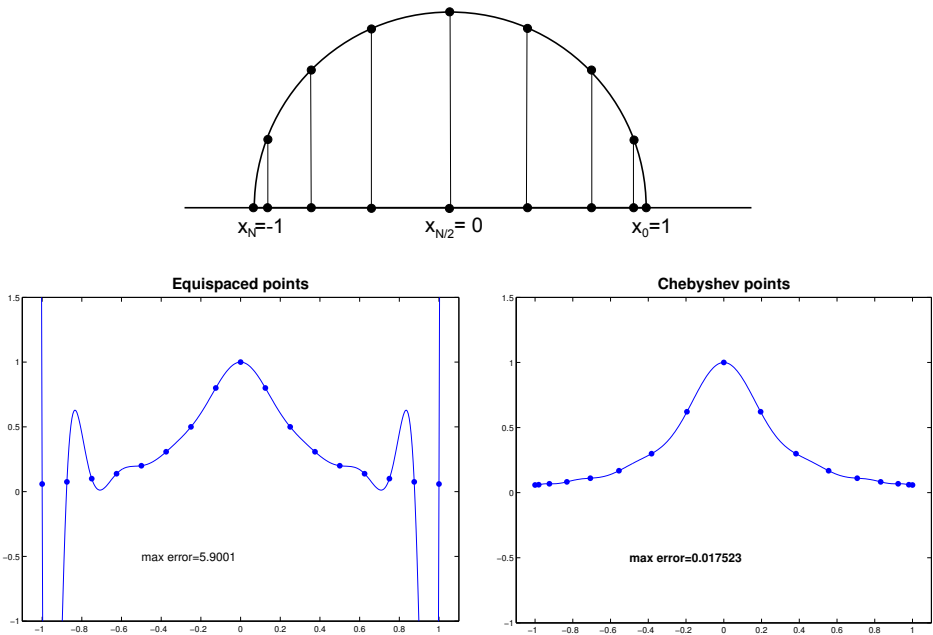


Figure 2. Top: Chebyshev points. Bottom: Chebyshev versus equispaced points.

Spectral methods have an exponential order of error convergence, so the error decreases much more rapidly than in other numerical methods. By increasing N , defined as the number of Chebyshev points, linearly, the error converges exponentially as in Figure 3 (reproduced from [Trefethen 2000]). However with finite differences method, the number of points are normally increased by a factor of ten to gain just one more decimal point of accuracy.

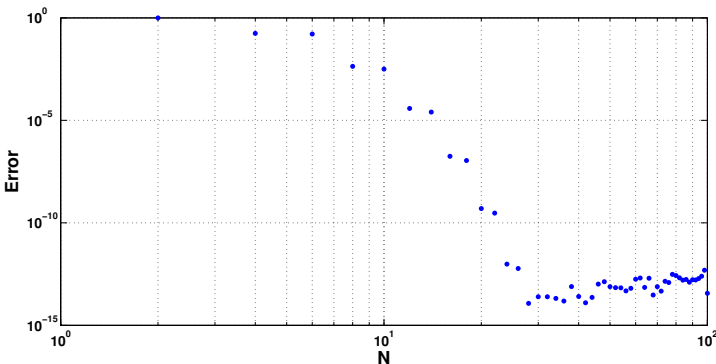


Figure 3. Convergence of spectral differentiation.

Choosing N . In order to find the most accurate solution, picking the correct number of Chebyshev points is imperative. As discussed earlier, as N is increased linearly the error decreases exponentially but only to a certain point. Eventually the error reaches a minimum and then begins to increase slowly due to machine error.

Claim 2.1. *For the reaction diffusion equation (5), the minimum error occurs at approximately $N = 14$.*

Proof. In order to select the optimal number of Chebyshev points, we calculate the error by comparing the exact solution of the linear form of (5) to the solution calculated with spectral methods. The linear form of (5) is

$$u_t = au_{xx} + u, \quad u(-1) = u(1) = 0. \tag{7}$$

By using the *separation of variables method*, we get the general solution of (7) as

$$u(x, t) = \sum_{n=1}^{\infty} c_n e^{(1-a/4(n\pi)^2)t} \sin(n\pi(x+1)/2). \tag{8}$$

If we pick our initial data as the eigenfunction $u(x, 0) = \sin(\pi(x+1)/2)$, we get $c_1 = 1$ and $c_n = 0$ for $n \geq 2$. So the exact solution of (7) with that initial data is

$$u(x, t) = e^{(1-a/4\pi^2)t} \sin(\pi(x+1)/2). \tag{9}$$

The approximate solution of (7) derived from the spectral methods:

$$u(x, t) = u_0 e^{At},$$

where $A = aD^2 + 1$, $u_0 = \sin \pi(x+1)/2$ and D^2 is the Chebyshev matrix derived by spectral methods.

Now we define the error as

$$\begin{aligned} \text{Error} &= \|\text{Exact solution} - \text{Approximate solution}\| \\ &= \left\| \left(e^{(1-a/4\pi^2)t} - e^{(aD^2+1)t} \right) \sin(\pi(x+1)/2) \right\|. \end{aligned}$$

where $\|\cdot\|$ represents the Euclidean norm. In Figure 4, for various a values, we observe that the error reaches its minimum at approximately $N = 14$. □

Claim 2.2. *For the Klein–Gordon equation (6), the minimum error occurs at approximately $N = 12$.*

Proof. Similar to what we did for the reaction-diffusion equation, we calculate the error by comparing the exact solution of the linear form of (6) to the solution calculated with spectral methods. The linear form of (6) is

$$u_{tt} + cu_t = au_{xx} + u, \quad u(-1) = u(1) = 0. \tag{10}$$

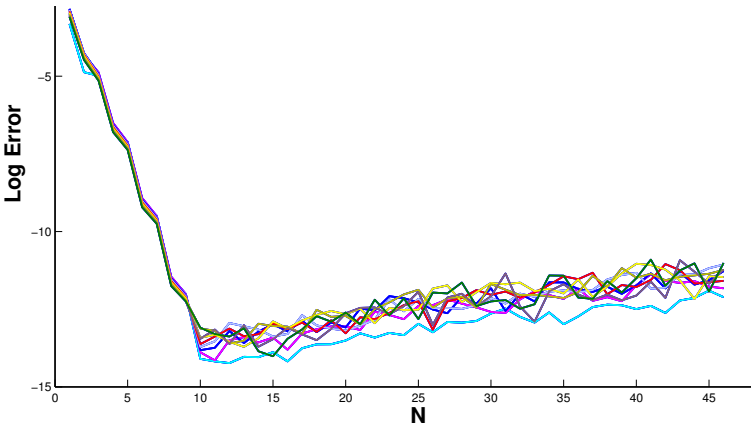


Figure 4. Error plots for a -values from 0.02 to 0.4.

By using the *separation of variables method* and picking the initial data as

$$u(x, 0) = \sin \frac{\pi(x + 1)}{2} \tag{11}$$

and

$$u_t(x, 0) = \left(-\frac{c}{2} + \sqrt{\frac{c^2}{4} + 1 - \frac{a}{4}\pi^2} \right) \sin \frac{\pi(x + 1)}{2} \tag{12}$$

and assuming $c^2 + 4 - a\pi^2 > 0$, we get the exact solution of (10) as

$$u(x, t) = \sin \left(\frac{\pi(x + 1)}{2} \right) \exp \left(\left(-\frac{c}{2} + \sqrt{\frac{c^2}{4} + 1 - \frac{a}{4}\pi^2} \right) t \right). \tag{13}$$

The approximate solution of (10) derived from the spectral methods is found by using ODE45 by changing the second order differential equation

$$u_{tt} + cu_t = au_{xx} + u = (aD^2 + 1)u$$

into a first order system y , defining $z := u_t$,

$$\begin{bmatrix} u \\ z \end{bmatrix}_t = \begin{bmatrix} 0 & I \\ aD^2 + I & -c \end{bmatrix} \begin{bmatrix} u \\ z \end{bmatrix}$$

and using the same initial conditions (11) and (12). We define the error same as we defined for the reaction-diffusion equation and use the Euclidean norm. **Figure 5** shows the error for various a values and fixed $c = 1$ (top), an for various c values and fixed $a = 0.1$ (bottom); we observe that the error reaches its minimum at approximately $N = 12$. □

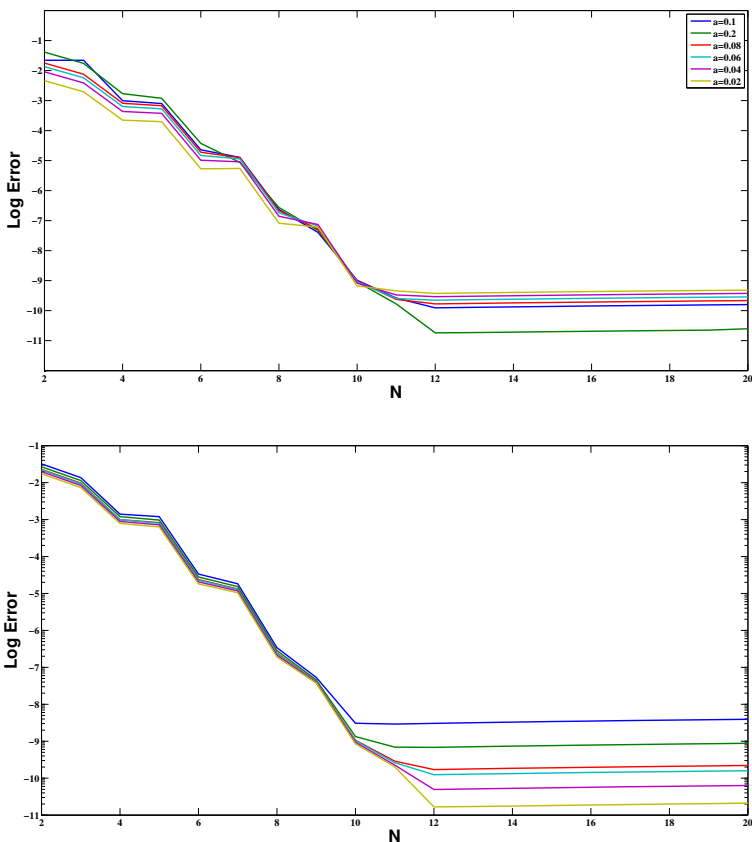


Figure 5. Log error. Top: $c = 1$, values of a from 0.02 to 0.2. Bottom: $a = 0.1$, values of c from 0.1 to 2.

3. Numerical existence of steady state solutions

Steady state solutions. For both equations, the reaction-diffusion (5) and the Klein–Gordon equation (6), the steady state solutions $u(x, t) = \phi(x)$ satisfy the same equation

$$-a\phi'' - \phi + \phi^3 = 0, \quad \phi(-1) = \phi(1) = 0 \tag{14}$$

since $\phi_t = 0$ and $\phi_{tt} = 0$. Figure 6 shows the steady state solutions for three different a -values, $a = 0.2$, $a = 0.1$ and $a = 0.03$. Consecutively (14) has 3, 5 and 7 solutions. The numerical computations show that as a is decreased, two new steady states of opposite sign and increasing number of oscillations occur for each bifurcation. The relation between a and number of steady state solutions will be analytically studied on page 731.

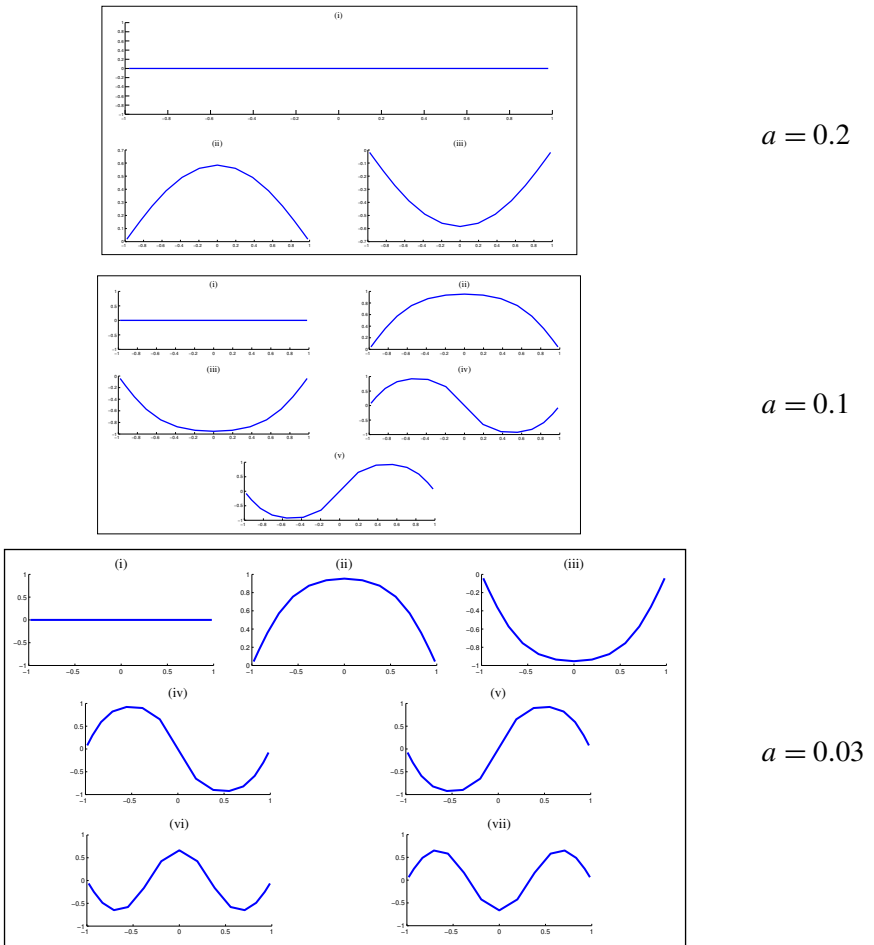


Figure 6. Steady state solutions for various values of a .

Note that zero is the trivial steady state solution for any a . For nonzero solutions, throughout this paper, we will name the steady state solutions. For example, we will name each convex steady state solution in Figure 6 an “n” solution — see graphs labeled (ii); each concave solution a “u” solution — graphs labeled (iii); graphs labeled (iv) for $a = 0.1$ and $a = 0.03$ are the “nu” solutions, and so on.

Bifurcations. The number of steady states for a given a value was verified with the shooting method. In Figure 7 we see shooting method plots for three a values. The number of solutions at an a value is the number of times the plot of $\phi(1)$ versus $\phi'(-1)$ touches the $\phi'(-1)$ axis where $\phi(1) = 0$. The bifurcation values to five decimal places were determined by changing a until a new number of solutions was observed. These bifurcation values are confirmed in the next subsection.

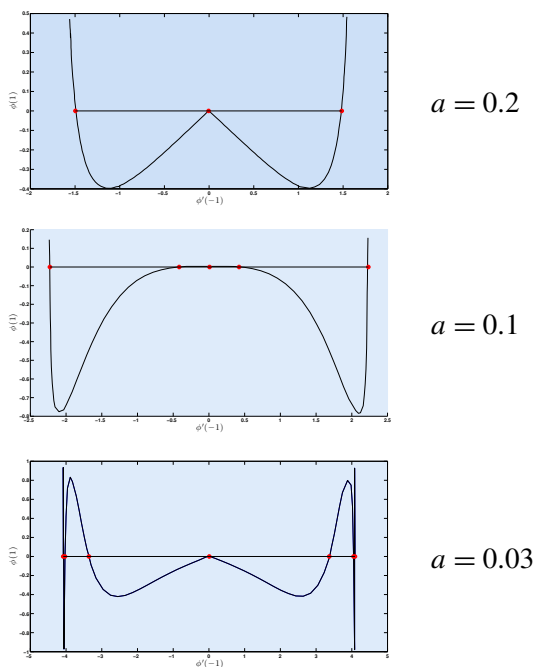


Figure 7. Existence of steady states $\phi(1)$ vs $\phi'(-1)$, for various values of a .

Determination of bifurcation values. In Section 3 and in the preceding subsection, the steady state solutions to both the nonlinear reaction diffusion equation (5) and the nonlinear Klein–Gordon equation (6) were calculated numerically, and the number of solutions were found for three a values. In particular it was found that for $a = 0.2$ there are three steady state solutions, for $a = 0.1$ there are five steady state solutions and for $a = 0.03$ there are seven steady state solutions.

In this section we find all bifurcation values for the parameter a ; at each value two new solutions are added. We will show that these bifurcations values are at $a = (2/n\pi)^2$ for n a positive integer. Thus the first few values are 0.4053, 0.1013, 0.0450, 0.0253; for $a > 0.4503$ there is only the zero solution, for $0.1013 < a < 0.4503$ there are three solutions, for $0.0450 < 0.1013$ there are five solutions, for $0.0253 < a < 0.0450$ there are seven solutions, and so on. This is consistent with the numerical results.

Consider the initial value problem

$$x' = y, \quad y' = -\lambda^2(x - x^3), \quad x(-1) = 0, \quad y(-1) = y_0, \quad (15)$$

which is equivalent to equations (14) with $1/\lambda^2$ substituted for a .

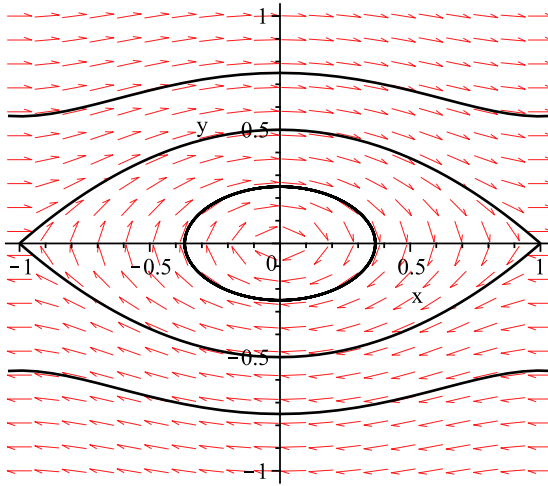


Figure 8. Phase portrait for $x' = y, y' = -\lambda^2(x - x^3)$ with $\lambda = 0.5$.

Clearly this system has saddle points at $(\pm 1, 0)$. Due to the symmetry of the vector field for this system, the fixed point at $(0, 0)$ is a center. Solution curves closer to the origin than the stable manifolds of $(\pm 1, 0)$ form closed loops. Thus the solution curves to (15) circle the origin in the clockwise direction for y_0 sufficiently small. See Figure 8.

Let $(x(y_0, t), y(y_0, t))$ represent the solution to (15) and let $\theta(y_0, t)$ represent the angle that the line segment connecting $(x(y_0, t), y(y_0, t))$ with $(0, 0)$ makes with the positive x -axis. Thus $\theta(y_0, t)$ is the angle in the polar coordinate representation of $(x(y_0, t), y(y_0, t))$, and hence $\tan \theta(y_0, t) = y(y_0, t)/x(y_0, t)$. Assume that θ starts at $\pi/2$, corresponding to the initial condition given in (15), and continues to decrease as the solution curve moves clockwise around the origin. Thus after one loop of the solution curve around the origin θ is $-\pi/2$, after two loops θ is $-3\pi/2$, and so on.

Theorem 3.1. $\theta(y_0, t)$ is an increasing function of $y_0 > 0$ for fixed t .

Proof. For convenience we suppress the y_0 argument and write $\theta(y_0, t)$ as $\theta(t)$. Differentiating $\tan \theta(t) = y(t)/x(t)$ with respect to t we get

$$(1 + \tan^2 \theta(t))\theta'(t) = \frac{y'(t)x(t) - y(t)x'(t)}{x^2(t)}.$$

Solving for $\theta'(t)$ and using $\tan^2 \theta(t) = y(t)^2/x(t)^2$ results in

$$\theta'(t) = \frac{y'(t)x(t) - y(t)x'(t)}{x^2(t) + y^2(t)}.$$

Then using the DE system $x' = y$, $y' = -\lambda^2(x - x^3)$ we get

$$\theta'(t) = \frac{-\lambda^2 x^2(t) + \lambda^2 x^4(t) - y^2(t)}{x^2(t) + y^2(t)}.$$

Switching to polar coordinates ($x = r \cos \theta$, $y = r \sin \theta$, $r^2 = x^2 + y^2$) on the right side yields

$$\begin{aligned} \theta'(t) &= \frac{-\lambda^2 r^2(t) \cos^2 \theta(t) + \lambda^2 r^4(t) \cos^4 \theta(t) - r^2(t) \sin^2 \theta}{r^2(t)} \\ &= -\lambda^2 \cos^2 \theta(t) + \lambda^2 r^2(t) \cos^4 \theta(t) - \sin^2 \theta(t). \end{aligned}$$

Rearranging a bit we get

$$\theta'(t) = \lambda^2 \cos^2 \theta(t) (-1 + r^2(t) \cos^2 \theta(t)) - \sin^2 \theta(t). \quad (16)$$

Using $x = r \cos \theta$ we could also write (16) as

$$\theta'(t) = \lambda^2 \cos^2 \theta(t) (-1 + x^2(t)) - \sin^2 \theta(t), \quad (17)$$

which shows that $\theta' < 0$ for $-1 < x < 1$. This is to be expected as we know that solution curves inside the unstable manifold of the fixed points circle the origin clockwise.

It is clear from (16) that θ' increases as a function of r for fixed θ . Since θ' is negative this means that for a given θ , the solution curves farther from the origin are circling the origin at a slower angular rate (smaller absolute value) than those that are closer. See Figure 9.

This implies that for y_0 chosen so that the solution curve forms a closed loop, smaller y_0 means that the solution curve has wrapped further around the origin in the clockwise direction, and hence $\theta(y_0, t)$ is smaller (for fixed t). This means $\theta(y_0, t)$ is an increasing function of y_0 as claimed.

Let $\lambda > 0$ be fixed. Let $x_1(y_0, t)$ represent the solution to

$$x' = y, \quad y' = -\lambda^2 x, \quad x(-1) = 0, \quad y(-1) = y_0. \quad (18)$$

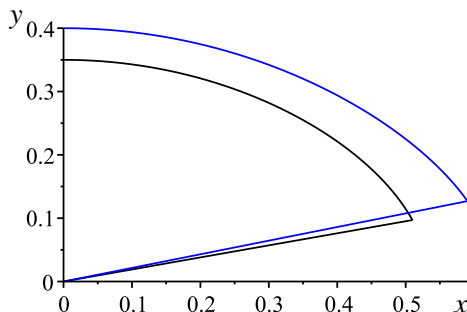


Figure 9. Solution curves closer to the origin move faster.

This is just (15) without the x^3 term. It is easy to show that

$$x_1(y_0, t) = y_0 \sin(\lambda(t+1))/\lambda \quad \text{and} \quad y_1(y_0, t) = y_0 \cos(\lambda(t+1)).$$

As before, let (r_1, θ_1) be the polar representation of (x_1, y_1) , so that $\theta_1(y_0, t)$ is the polar angle for the point $(x_1(y_0, t), y_1(y_0, t))$. Since

$$\tan \theta_1(y_0, t) = \frac{y_1(y_0, t)}{x_1(y_0, t)} = \frac{y_0 \cos(\lambda(t+1))}{y_0 \sin(\lambda(t+1))/\lambda} = \lambda \cot(\lambda(t+1)),$$

we know that $\theta_1(y_0, t)$ is in fact independent of y_0 . Thus instead of $\theta_1(y_0, t)$ we will write $\theta_1(t)$. \square

Theorem 3.2. Fix t and λ . As $y_0 \rightarrow 0$, $\theta(y_0, t) \rightarrow \theta_1(t)$ monotonically.

Proof. The monotonic part follows from the previous theorem. To prove the limit part, the basic idea is that x^3 is negligible compared to x for small x , and so the linear and nonlinear vector fields, given in Equations (15) and (18), respectively, are indistinguishable for small x . We now flesh out the details of this argument.

For the IVP, $x'' + \lambda^2(x - x^3) = 0$, $x(-1) = 0$, $x'(-1) = y_0$, which is just (15) written in second-order form, we can multiply the DE by x' to get

$$x'x'' + \lambda^2(x - x^3)x' = 0.$$

We can integrate both sides now to get

$$\frac{1}{2}(x')^2 + \lambda^2\left(\frac{1}{2}x^2 - \frac{1}{4}x^4\right) = C.$$

Then using $x(-1) = 0$ and $x'(-1) = y_0$ we get $C = y_0^2/2$. We now have

$$(x')^2 + \lambda^2\left(x^2 - \frac{1}{2}x^4\right) = y_0^2 \tag{19}$$

after substituting and multiplying by 2. Plotting (19) in the phase plane (x on the horizontal axis and x' on the vertical) for various y_0 we are back to the closed curves in Figure 8, which shows clearly that $x(t)$ can be “trapped” in an arbitrarily small region $-\varepsilon < x(t) < \varepsilon$ if y_0 is taken to be sufficiently small. \square

In order to finish the proof of the theorem we need to invoke a version of the Gronwall inequality:

Lemma 3.3 (Gronwall’s inequality: see for example [Howard 1998, Theorem 2.1]). Let X be a Banach space and $U \subset X$ an open set in X . Let $f, g : [a, b] \times U \rightarrow X$ be continuous functions and let $y, z : [a, b] \rightarrow U$ satisfy the initial value problems

$$\begin{aligned} y'(t) &= f(t, y(t)), & y(a) &= y_0 \\ z'(t) &= g(t, z(t)), & z(a) &= z_0. \end{aligned} \tag{20}$$

Also assume there is a constant $C \geq 0$ so that

$$\|g(t, x_2) - g(t, x_1)\| \leq C \|x_2 - x_1\| \quad (21)$$

and a continuous function $\phi : [a, b] \rightarrow [0, \infty)$ so that

$$\|f(t, y(t)) - g(t, y(t))\| \leq \phi(t). \quad (22)$$

Then for $t \in [a, b]$

$$\|y(t) - z(t)\| \leq e^{C|t-a|} \|y_0 - z_0\| + e^{C|t-a|} \int_a^t e^{-C|s-a|} \phi(s) ds.$$

For our purposes the Banach space X is just the real numbers, so that the norm is the absolute value.

For convenience we suppress the y_0 and write $\theta(t)$ instead of $\theta(y_0, t)$. We can rewrite (17) as

$$\theta'(t) = f(t, \theta(t)),$$

where

$$f(t, \theta) = -\lambda^2 \cos^2 \theta - \sin^2 \theta + \lambda^2 x^2(t) \cos^2 \theta$$

and where $x(t)$ comes from the solution to the full system in (15). Similarly, θ_1 satisfies

$$\theta_1'(t) = g(t, \theta_1(t)),$$

where

$$g(t, \theta) = -\lambda^2 \cos^2 \theta - \sin^2 \theta.$$

We now apply the Gronwall inequality using the above choices for f and g , where the interval $[a, b]$ is $[-1, 1]$ and where we choose the same initial condition $\pi/2$ for the DEs, that is, $\theta(-1) = \pi/2$ and $\theta_1(-1) = \pi/2$ (which corresponds to $x(0) = 0$ and $y(0) = y_0$ in rectangular coordinates). Equation (21) is called a Lipschitz condition and is satisfied by $g(t, \theta)$ for some C because it is continuously differentiable as a function of θ . Finally since

$$|f(t, \theta(t)) - g(t, \theta(t))| = |\lambda^2 x^2(t) \cos^2 \theta(t)| \leq \lambda^2 x^2(t),$$

we see that (22) is satisfied with $\phi(t) = \lambda^2 x^2(t)$. The conclusion of the Gronwall inequality follows, which means that for fixed $t \in [-1, 1]$ and λ

$$|\theta(t) - \theta_1(t)| \leq e^{C|t+1|} \int_{-1}^t e^{-C|s+1|} \lambda^2 x^2(s) ds$$

since the initial conditions are the same. If we assume that $|x(t)| < \varepsilon$ then

$$\begin{aligned} e^{C|t+1|} \int_{-1}^t e^{-C|s+1|} \lambda^2 x^2(s) ds &< e^{C|t+1|} \int_{-1}^t e^{-C|s+1|} \lambda^2 \varepsilon^2 ds \\ &= \frac{1}{C} \lambda^2 \varepsilon^2 (e^{C|t+1|} - 1). \end{aligned}$$

Following the above inequalities we have shown that

$$|\theta(y_0, t) - \theta_1(t)| < \frac{1}{C} \lambda^2 \varepsilon^2 (e^{C|t+1|} - 1).$$

The theorem follows by recalling that $|x(t)|$ can be made arbitrarily small for y_0 sufficiently small.

Theorem 3.4. *The eigenvalues of the linear BVP*

$$x'' + \lambda^2 x = 0, \quad x(-1) = 0, \quad x(1) = 0 \quad (23)$$

are the bifurcation points for the nonlinear BVP

$$x'' + \lambda^2(x - x^3) = 0, \quad x(-1) = 0, \quad x(1) = 0. \quad (24)$$

Specifically the eigenvalues of the linear problem are $\lambda_n = n\pi/2$, and there is one solution to the nonlinear problem (the zero solution) for $0 \leq \lambda \leq \lambda_1$, three solutions to the nonlinear problem for $\lambda_1 < \lambda \leq \lambda_2$, five solutions to the nonlinear problem for $\lambda_2 < \lambda \leq \lambda_3$, and so on.

Proof. If λ_n is an eigenvalue for the BVP in (23) it is easy to show that $\lambda_n = n\pi/2$ for $n = 1, 2, \dots$ and that the corresponding eigenfunctions are any multiple of $\sin(\lambda_n(t+1))$. Note that the system of differential equations in (18) is equivalent to the differential equation in (23). Thus if $\lambda = \lambda_n$ for some $n \geq 1$, then a solution to (18) automatically satisfies $x(1) = 0$ and so is a solution to (23) for any y_0 . This explains the relationship between the IVP in (18) and the BVP in (23).

The relationship between the nonlinear IVP in (15) and the nonlinear BVP in (24) is similar in that the differential equations are equivalent. However, because of the nonlinearity, (24) can be solved for *any* λ by solving the IVP in (15) and varying y_0 until $x(1) = 0$ is obtained (sometimes called the “shooting method” for solving a BVP). Note that $x(1) = 0$ in the phase plane means that the angle $\theta(y_0, 1)$ is any of $-\pi/2, -3\pi/2, -5\pi/2, \dots$

Now fix λ and start with y_0 chosen so that the solution to the IVP in (15) is the stable manifold of $(1, 0)$. As y_0 decreases towards zero, $\theta(y_0, 1)$ will wrap clockwise around the origin until it reaches $\theta_1(1)$ in the limit, as shown in the previous theorem. Every time $\theta(y_0, 1)$ passes $-\pi/2$ for n odd we get a solution to the nonlinear BVP in (24). If $\lambda < \lambda_1$ this never happens (because $\theta_1(1) > -\pi/2$), so the only solution is the zero solution. If $\lambda_1 < \lambda < \lambda_2$ then $-3\pi/2 < \theta_1(y_0, 1) < -\pi/2$

and so $\theta(y_0, 1)$ will pass just $-\pi/2$, in which case we have the zero solution as well as one more solution. By symmetry, a third solution occurs for y_0 negative. If $\lambda_2 < \lambda < \lambda_3$, then $\theta(y_0, 1)$ will pass $-\pi/2$ and $-3\pi/2$ yielding two solutions, plus the zero solution, plus the symmetric solutions for y_0 negative, for a total of five. Proceeding in this manner, the theorem is proved. \square

As stated earlier in this section, we have substituted $1/\lambda^2$ for the parameter a in the nonlinear reaction-diffusion and Klein-Gordon equations, and thus the bifurcation values in terms of a are $a = (2/n\pi)^2$.

4. Stability analysis

In order to determine the stability of a steady state solution, we look at the solution in the vicinity of the steady state and observe its behavior over time.

We assume that $u(x, t)$ is the solution such that $u_0 = u(x, 0)$ is in the vicinity of the steady state solution. The difference between the solution and steady state solution is known as the perturbation and is denoted as $v(x, t)$ and, satisfies

$$v(x, t) = u(x, t) - \phi(x). \tag{25}$$

Stability analysis will require us to study the long time behavior of the perturbation. If the solution diverges from the steady state ($\lim_{t \rightarrow \infty} \|v\| \rightarrow \infty$), then the steady state is unstable. If the solution does not diverge and the perturbation remains small, the steady state is stable.

Stability of reaction-diffusion equation. By substituting (25) into (5), we get

$$(\phi + v)_t - a(\phi + v)_{xx} - (\phi + v) + (\phi + v)^3 = 0.$$

Since $-a\phi'' - \phi + \phi^3 = 0$ and $\phi_t = 0$, we get

$$v_t - av_{xx} - v + 3\phi^2v + 3\phi v^2 + v^3 = 0.$$

By stability manifold theorem, we can say that the stability of the above equation will be similar to its linearized equation which is as follows:

$$v_t - av_{xx} - v + 3\phi^2v = 0,$$

which can be rewritten as

$$v_t = (aD^2 + 1 - 3\phi^2)v = 0.$$

So the eigenvalues of the linearized RD operator $aD^2 + 1 - 3\phi^2$ will tell us if v blows up in time, decreases to 0, or stays bounded.

Our numerical results show that the largest eigenvalues of the linearized RD operator about the “u” and “n” solutions are negative. This implies that these

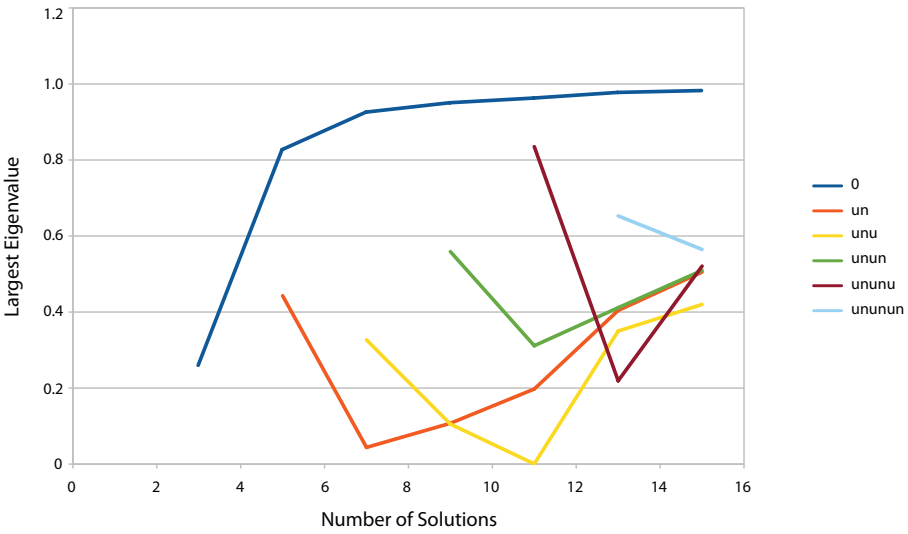


Figure 10. Largest eigenvalue of the linearized RD operator for the unstable steady states.

solutions are stable. All other solutions are unstable because the linearized RD operator has at least one positive eigenvalue. Figure 10 shows the largest eigenvalue of the linearized RD operator about each unstable steady state as the number of solutions from a given a -value increases (as the a -value decreases).

Stability of Klein–Gordon equation. By substituting (25) into (6), we get

$$(\phi + v)_{tt} + c(\phi + v)_t - a(\phi + v)_{xx} - (\phi + v) + (\phi + v)^3 = 0.$$

Since $-a\phi'' - \phi + \phi^3 = 0$, and $\phi_t = 0$ and $\phi_{tt} = 0$, we get

$$v_{tt} - av_{xx} - v + 3\phi^2v + 3\phi v^2 + v^3 = 0.$$

By the stable manifold theorem, we can say that the stability of the above equation will be similar to its linearized equation, which is as follows:

$$v_{tt} + cv_t - av_{xx} - v + 3\phi^2v = 0.$$

Let’s write it as a first order system by defining $v_t = w$. We get

$$\begin{bmatrix} v \\ w \end{bmatrix}_t = \begin{bmatrix} 0 & I \\ aD^2 + I - 3\phi^2 & -c \end{bmatrix} \begin{bmatrix} v \\ w \end{bmatrix}.$$

So we need to find the eigenvalues of the operator matrix in this equation in order to find the long time behavior of $\begin{bmatrix} v \\ w \end{bmatrix}$.

Because all of the new steady states that occur after three solutions are unstable, we then look at how unstable they are. One metric for instability is the magnitude

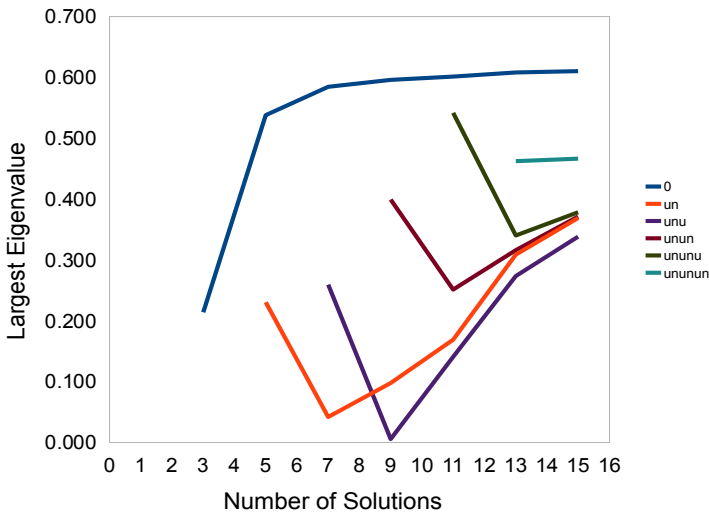


Figure 11. Largest eigenvalue of the linearized KG operator for the unstable steady states.

of the largest positive eigenvalue. The larger this eigenvalue is, the more unstable the steady state. Figure 11 shows the magnitude of the largest positive eigenvalue for various solutions as the number of solutions from a given a -value increases (as the a -value decreases). Note how the solution becomes more stable at first, and then becomes less stable as a decreases. Also note that the zero solution becomes more unstable quickly but then approaches a level of instability asymptotically.

In Figure 12, steady states are indicated stable or unstable and are organized by the bifurcation range that they occur in (number of solutions for a range of values

	Number of Solutions							
0	1	3	5	7	9	11	13	15
~	stable	unstable	unstable	unstable	unstable	unstable	unstable	unstable
~		stable	stable	stable	stable	stable	stable	stable
~		stable	stable	stable	stable	stable	stable	stable
~			unstable	unstable	unstable	unstable	unstable	unstable
~			unstable	unstable	unstable	unstable	unstable	unstable
~				unstable	unstable	unstable	unstable	unstable
~				unstable	unstable	unstable	unstable	unstable
~					unstable	unstable	unstable	unstable
~						unstable	unstable	unstable
~							unstable	unstable
~								unstable
~								unstable

Figure 12. The stability of different types of solutions as the value of a decreases.

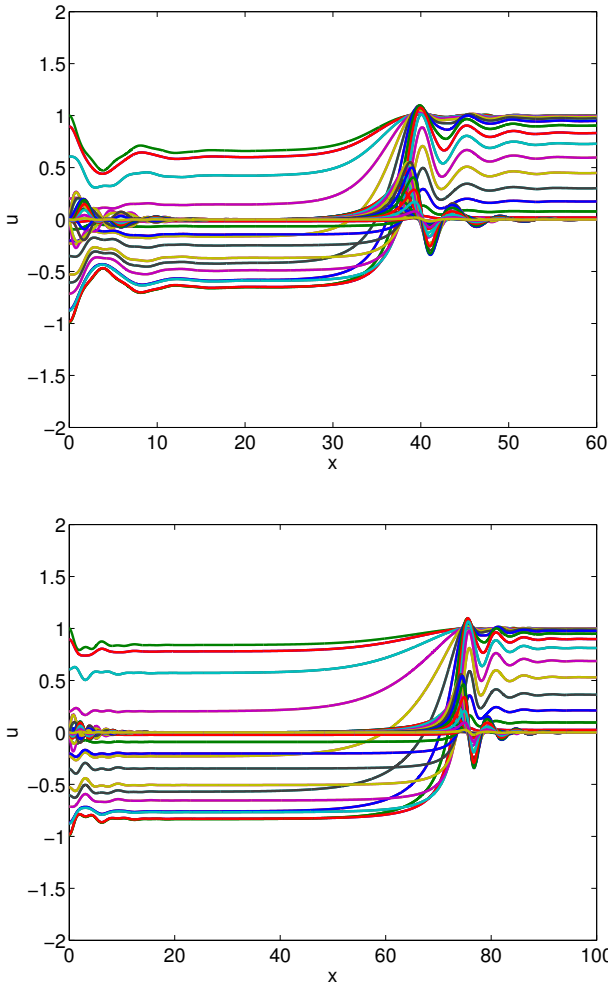


Figure 13. Side-view plots. Top: $a = 0.03$, $c = 0.5$. Bottom: $a = 0.02$, $c = 0.5$.

of a) and the look of the solution. For a values with only one steady state, the only steady state is the zero solution and it is stable. For all other bifurcation ranges, the zero solution is unstable. The solutions depicted in the second and third row of Figure 12 are stable. All other steady states are unstable.

In Figure 13 we compare two side-view plots to verify that the increase in stability of unstable steady states as observed in Figure 11 actually happens. As expected, the side plot with $a = 0.02$ (9-solution range) took longer to move to a stable solution than the plot with $a = 0.03$ (7-solution range) because it was less unstable (the positive eigenvalues were closer to being negative).

5. Simulations

Figure 14 depicts simulations of the Klein-Gordon equation for the comparison made in the previous section between $a = 0.03$ and $a = 0.02$ with $c = 0.5$. The simulation with $a = 0.02$ takes longer than the simulation with $a = 0.03$ to reach a stable steady state solution. These images agree with the side-view plots in Figure 13 and the plot in Figure 11. The simulations can be seen at youtu.be/dlNnTOUUMX8 ($a = 0.02$) and youtu.be/ccdF6tU2Vcw ($a = 0.03$).

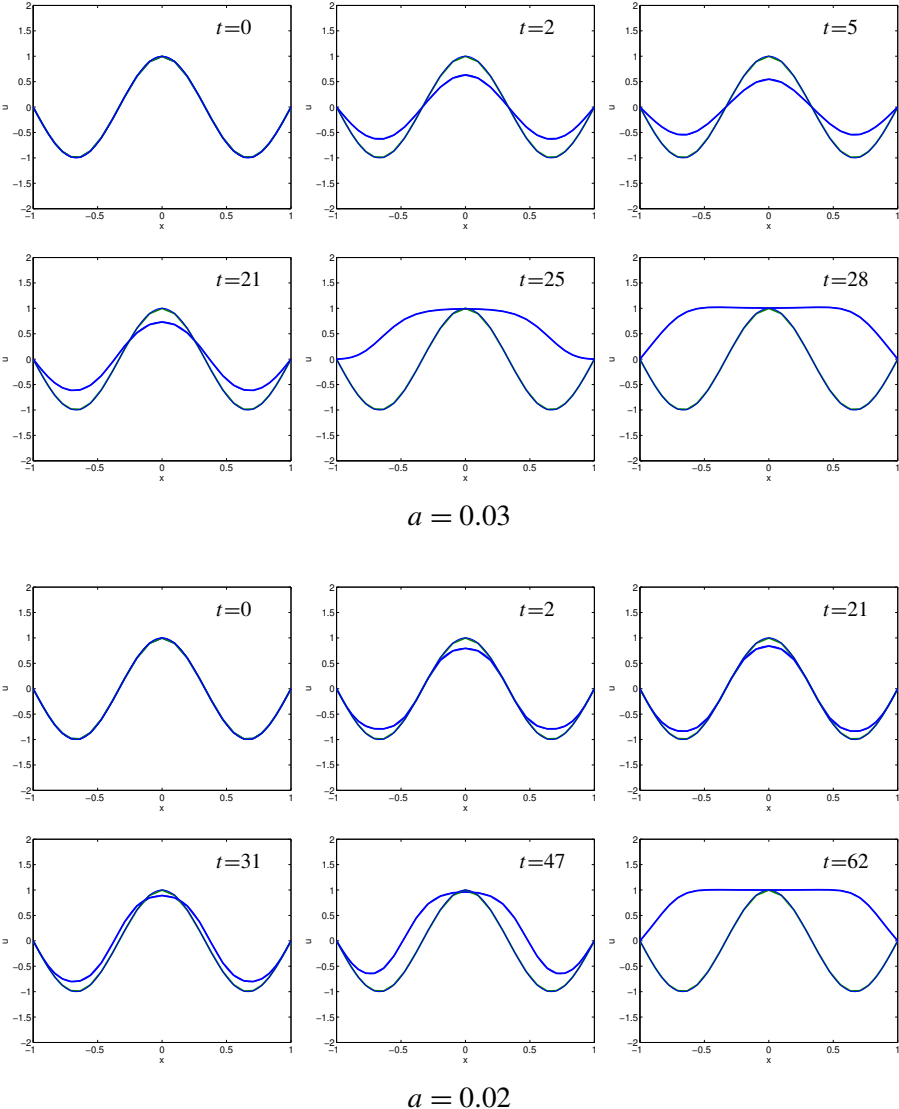


Figure 14. Results of the simulations for $a = 0.03$ and $a = 0.02$.

References

- [Howard 1998] R. Howard, “The Gronwall inequality”, lecture notes, 1998, available at <http://www.math.sc.edu/~howard/Notes/gronwall.pdf>.
- [Khain et al. 2010] E. Khain, Y. T. Lin, and L. M. Sander, “Fluctuations and stability in front propagation”, preprint, 2010. [arXiv 1009.5945v1](https://arxiv.org/abs/1009.5945v1)
- [Trefethen 2000] L. N. Trefethen, *Spectral methods in MATLAB*, Software, Environments, and Tools **10**, Society for Industrial and Applied Mathematics, Philadelphia, 2000. [MR 2001c:65001](#) [Zbl 0953.68643](#)

Received: 2012-12-05

Revised: 2013-10-29

Accepted: 2013-11-05

Miles.Aron@uzh.ch

University of Zurich, Sonneggstrasse 23, CH-8006 Zurich, Switzerland

pbowers@fas.harvard.edu

Harvard University, 230 Chestnut Street, Cambridge, MA 02139, United States

nicole_byer@brown.edu

Brown University, 45 Prospect Street, Providence, RI 02912, United States

rdecker@hartford.edu

University of Hartford, 200 Bloomfield Ave, West Hartford, CT 06117, United States

demirkaya@hartford.edu

University of Hartford, Dano Hall 210, 200 Bloomfield Ave, West Hartford, CT 06117, United States

junhwan.ryu@yale.edu

Yale University, 206 Elm Street #205495, New Haven, CT 06520-5495, United States

EDITORS

MANAGING EDITOR

Kenneth S. Berenhaut, Wake Forest University, USA, berenhks@wfu.edu

BOARD OF EDITORS

Colin Adams	Williams College, USA colin.c.adams@williams.edu	David Larson	Texas A&M University, USA larson@math.tamu.edu
John V. Baxley	Wake Forest University, NC, USA baxley@wfu.edu	Suzanne Lenhart	University of Tennessee, USA lenhart@math.utk.edu
Arthur T. Benjamin	Harvey Mudd College, USA benjamin@hmc.edu	Chi-Kwong Li	College of William and Mary, USA ckli@math.wm.edu
Martin Bohner	Missouri U of Science and Technology, USA bohner@mst.edu	Robert B. Lund	Clemson University, USA lund@clemson.edu
Nigel Boston	University of Wisconsin, USA boston@math.wisc.edu	Gaven J. Martin	Massey University, New Zealand g.j.martin@massey.ac.nz
Amarjit S. Budhiraja	U of North Carolina, Chapel Hill, USA budhiraj@email.unc.edu	Mary Meyer	Colorado State University, USA meyer@stat.colostate.edu
Pietro Cerone	La Trobe University, Australia P.Cerone@latrobe.edu.au	Emil Minchev	Ruse, Bulgaria eminchev@hotmail.com
Scott Chapman	Sam Houston State University, USA scott.chapman@shsu.edu	Frank Morgan	Williams College, USA frank.morgan@williams.edu
Joshua N. Cooper	University of South Carolina, USA cooper@math.sc.edu	Mohammad Sal Moslehian	Ferdowsi University of Mashhad, Iran moslehian@ferdowsi.um.ac.ir
Jem N. Corcoran	University of Colorado, USA corcoran@colorado.edu	Zuhair Nashed	University of Central Florida, USA znashed@mail.ucf.edu
Toka Diagana	Howard University, USA tdiagana@howard.edu	Ken Ono	Emory University, USA ono@mathcs.emory.edu
Michael Dorff	Brigham Young University, USA mdorff@math.byu.edu	Timothy E. O'Brien	Loyola University Chicago, USA tbriell@luc.edu
Sever S. Dragomir	Victoria University, Australia sever@matilda.vu.edu.au	Joseph O'Rourke	Smith College, USA orourke@cs.smith.edu
Behrouz Emamizadeh	The Petroleum Institute, UAE bemamizadeh@pi.ac.ae	Yuval Peres	Microsoft Research, USA peres@microsoft.com
Joel Foisy	SUNY Potsdam foisyjs@potsdam.edu	Y.-F. S. Pétermann	Université de Genève, Switzerland petermann@math.unige.ch
Errin W. Fulp	Wake Forest University, USA fulp@wfu.edu	Robert J. Plemmons	Wake Forest University, USA rplemmons@wfu.edu
Joseph Gallian	University of Minnesota Duluth, USA kgallian@d.umn.edu	Carl B. Pomerance	Dartmouth College, USA carl.pomerance@dartmouth.edu
Stephan R. Garcia	Pomona College, USA stephan.garcia@pomona.edu	Vadim Ponomarenko	San Diego State University, USA vadim@sciences.sdsu.edu
Anant Godbole	East Tennessee State University, USA godbole@etsu.edu	Bjorn Poonen	UC Berkeley, USA poonen@math.berkeley.edu
Ron Gould	Emory University, USA rg@mathcs.emory.edu	James Propp	U Mass Lowell, USA jpropp@cs.uml.edu
Andrew Granville	Université Montréal, Canada andrew@dms.umontreal.ca	József H. Przytycki	George Washington University, USA przytyck@gwu.edu
Jerrold Griggs	University of South Carolina, USA griggs@math.sc.edu	Richard Rebarber	University of Nebraska, USA rrebarbe@math.unl.edu
Sat Gupta	U of North Carolina, Greensboro, USA sgupta@uncg.edu	Robert W. Robinson	University of Georgia, USA rwr@cs.uga.edu
Jim Haglund	University of Pennsylvania, USA jhaglund@math.upenn.edu	Filip Saidak	U of North Carolina, Greensboro, USA f_saidak@uncg.edu
Johnny Henderson	Baylor University, USA johnny_henderson@baylor.edu	James A. Sellers	Penn State University, USA sellersj@math.psu.edu
Jim Hoste	Pitzer College jhoste@pitzer.edu	Andrew J. Sterge	Honorary Editor andy@ajsterge.com
Natalia Hritonenko	Prairie View A&M University, USA nhritonenko@pvamu.edu	Ann Trenk	Wellesley College, USA atrenk@wellesley.edu
Glenn H. Hurlbert	Arizona State University, USA hurlbert@asu.edu	Ravi Vakil	Stanford University, USA vakill@math.stanford.edu
Charles R. Johnson	College of William and Mary, USA crjohnso@math.wm.edu	Antonia Vecchio	Consiglio Nazionale delle Ricerche, Italy antonia.vecchio@cnr.it
K. B. Kulasekera	Clemson University, USA kk@ces.clemson.edu	Ram U. Verma	University of Toledo, USA verma99@msn.com
Gerry Ladas	University of Rhode Island, USA gladas@math.uri.edu	John C. Wierman	Johns Hopkins University, USA wierman@jhu.edu
		Michael E. Zieve	University of Michigan, USA zieve@umich.edu

PRODUCTION


Silvio Levy, Scientific Editor

See inside back cover or msp.org/involve for submission instructions. The subscription price for 2014 is US \$120/year for the electronic version, and \$165/year (+\$35, if shipping outside the US) for print and electronic. Subscriptions, requests for back issues from the last three years and changes of subscribers address should be sent to MSP.

Involve (ISSN 1944-4184 electronic, 1944-4176 printed) at Mathematical Sciences Publishers, 798 Evans Hall #3840, c/o University of California, Berkeley, CA 94720-3840, is published continuously online. Periodical rate postage paid at Berkeley, CA 94704, and additional mailing offices.

Involve peer review and production are managed by EditFLOW[®] from Mathematical Sciences Publishers.

PUBLISHED BY

 **mathematical sciences publishers**
nonprofit scientific publishing

<http://msp.org/>

© 2014 Mathematical Sciences Publishers

involve

2014

vol. 7

no. 6

A median estimator for three-dimensional rotation data	713
MELISSA BINGHAM AND ZACHARY FISCHER	
Numerical results on existence and stability of steady state solutions for the reaction-diffusion and Klein–Gordon equations	723
MILES ARON, PETER BOWERS, NICOLE BYER, ROBERT DECKER, ASLIHAN DEMIRKAYA AND JUN HWAN RYU	
The h-vectors of PS ear-decomposable graphs	743
NIMA IMANI, LEE JOHNSON, MCKENZIE KEELING-GARCIA, STEVEN KLEE AND CASEY PINCKNEY	
Zero-inflated Poisson (ZIP) distribution: parameter estimation and applications to model data from natural calamities	751
SADIE BECKETT, JOSHUA JEE, THAPELO NCUBE, SOPHIA POMPILUS, QUINTEL WASHINGTON, ANSHUMAN SINGH AND NABENDU PAL	
On commutators of matrices over unital rings	769
MICHAEL KAUFMAN AND LILLIAN PASLEY	
The nonexistence of cubic Legendre multiplier sequences	773
TAMÁS FORGÁCS, JAMES HALEY, REBECCA MENKE AND CARLEE SIMON	
Seating rearrangements on arbitrary graphs	787
DARYL DEFORD	
Fibonacci Nim and a full characterization of winning moves	807
CODY ALLEN AND VADIM PONOMARENKO	